Journal of
Materials Chemistry C

Materials for optical, magnetic and electronic devices

Accepted Manuscript

This article can be cited before page numbers have been issued, to do this please use: G. Di Carlo, A. Forni, P. Moretti, D. Marinotto, C. Botta, M. Pizzotti, F. Tessore and E. Cariati, *J. Mater. Chem. C*, 2021, DOI: 10.1039/D1TC00503K.

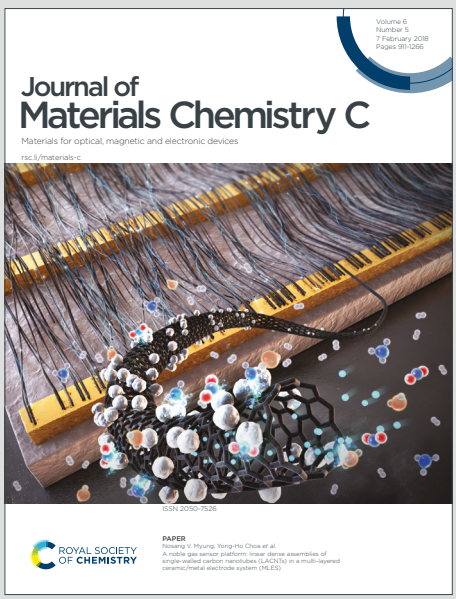

ROYAL SOCIETY OF CHEMISTRY

rsc.li/materials-c

View Article Online
DOI: 10.1039/D1TC00503K

ARTICLE

Combined Effects of Ion-Pairing on Multi-Emissive Properties of Benzimidazolium Salts

Received 00th January 20xx,
Accepted 00th January 20xx

DOI: 10.1039/x0xx00000x

Gabriele Di Carlo,*[a] Alessandra Forni,*[b] Paola Moretti,[a] Daniele Marinotto,[b] Chiara Botta,[c] Maddalena Pizzotti,[a] Francesca Tessore[a] and Elena Cariati [a]

The possibility to control luminescent properties of purely organic emitting salts is receiving an ever-growing interest. A full understanding of the manifold effects of counterions on the photophysics of charged luminophors deserves thorough investigation. Here, we disclose the impact of different anions, i.e. triflate, iodide and nitrate, on the multiple emissions of a new class of ionic luminophors, based on *1,3*-dimethyl-*2*-(p-tolyl)-*1H*-benzo[*d*]imidazol-*3*-ium, **1**. The specific ion-pairing plays a key role in the emissive features of the solids, depending on both the anion's electronegativity and the cation-anion distance. Three main effects emerge from strong ion-pairing: i) fluorescence quenching, ii) phosphorescence enhancement and iii) efficient direct population of triplet-state. As a result, a weak interaction (**1-OTf**) guarantees intense fluorescence (QY > 50%), while a strong pairing (**1-NO_3·0.5EtOH** and **1-I·0.5CH_2Cl_2**) promotes molecular room temperature phosphorescence (RTP) enhancement. The anion-controlling strategy also enables long-lasting RTP (288 ms) in **1-OTf** and ultrabright phosphorescence (QY > 70%) in **1-NO_3·0.5EtOH**, under direct triplet-excitation at 350 nm.

Introduction

To date purely organic compounds exhibiting room temperature luminescence in the solid state have made impressive strides as advanced optical materials for a wide range of potential applications.[1–3] The profitable properties, such as low-cost starting materials, rationally tailored molecular structures and good processability in mild condition, make them very attractive.[4–7] Molecular design,[2,8,9] crystal packing engineering,[10,11] co-crystallization[12] and heavy atom[13,14] are some viable strategies explored in the last decade to boost phosphorescence of light-emitting solids. The switch between fluorescence and phosphorescence emissions has been also precisely regulated through either external stimuli, such as mechanical forces and pH variation,[15,16] or molecular design.[17]
Very recently, a growing interest has emerged in designing organic salts as solid emitters with tunable photophysical properties by varying both cation[18] and anion constituents.[6-9] Variation of halides, as counterions, has been explored as a viable strategy to manipulate the photophysical properties of cationic emitters.[19,20] On one hand, the counter-ion of light-emitting salts may positively affect their crystal packing,[21] resulting in enhanced emissive properties by reducing non-radiative decay channels.[22] On the other hand, electronic coupling within ionic pairs is expected to influence the compound's photophysics. Stronger external heavy atom effect (EHE)[23] has been observed in halogen-substituted N-alkylcarbazole by varying the linker length and thus the halogen -luminophore distance. However, the impact of ion separation on organic salts showing unchanged ionic couple, to the best of our knowledge, has never been reported to date. Thus, more studies on the role of specific counterions require immediate attention in order to develop a strategy to control the optical properties of charged luminophores. This will open new ways to design advanced purely organic room temperature phosphorescent (RTP) materials with tunable emissions by simply varying the counterions.
In this work we report on the preparation and characterization of a new class of ionic luminogens, namely benzimidazolium salts, **1**, with triflate, nitrate and iodide counterions featuring different size and electronic nature. Four crystal structures are isolated depending on the relative anion and crystallization solvent producing two diverse nitrate crystals which differ in ion distancing. The resulting compounds exhibit multiple emissions in solid-state, spanning from fluorescence (FL) to molecular phosphorescence (PH_M) and supramolecular phosphorescence (PH_S). Both the distance and the nature of counterions are found to impact on the photophysical behavior by affecting both molecular and supramolecular features of **1**-salts. Spectroscopic studies along with theoretical investigations and structural analysis shed light on the role of ion-pairing, evidencing a threefold impact on the emissive behavior of **1**-salts: FL quenching, PH_M enhancing and direct excitation triggering of triplet-states.

[a] Department of Chemistry University of Milan and INSTM Research Unit. Via C. Golgi 19, 20133 Milan (Italy). E-mail: gabriele.dicarlo@unimi.it
[b] CNR-SCITEC, Istituto di Scienze e Tecnologie Chimiche "G. Natta". Via C. Golgi 19, 20133 Milan (Italy). E-mail: alessandra.forni@scitec.cnr.it
[c] CNR-SCITEC, Istituto di Scienze e Tecnologie Chimiche "G. Natta" Via A. Corti 12, 20133 MILANO (Italy)
†Electronic Supplementary Information (ESI) available: [details of any supplementary information available should be included here]. See DOI: 10.1039/x0xx00000x

Results and discussion

Synthetic procedures

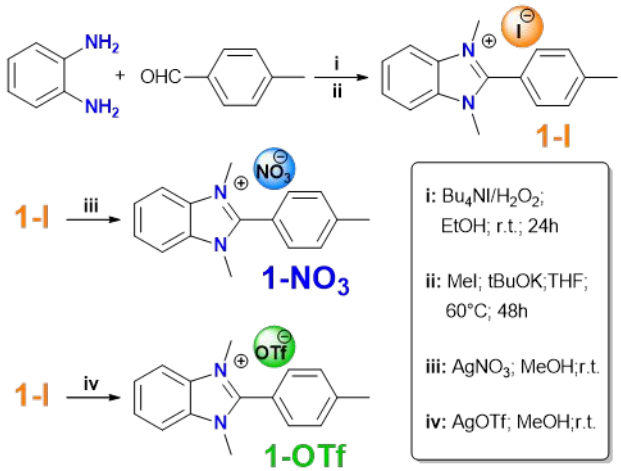

Scheme 1. Schematic synthetic procedure for preparation of **1-I**, **1-NO$_3$** and **1-OTf**.

The synthetic procedures for the preparation of triflate (**1-OTf**), nitrate (**1-NO$_3$**) and iodide (**1-I**) salts of 1,3-dimethyl-2-(4-methylphenyl)-1H-benzimidazolium (**1**) salts are trivial and occur with excellent yields under mild conditions (Scheme 1).[24] *o*-Phenylendiamine and *p*-Tolualdehyde in ethanol at room temperature undergo efficient (>90%) oxidative condensation (i) to give the benzimidazole core through hypervalent iodine generated *in-situ* from Bu_4NI/H_2O_2. The following double alkylation of nitrogen atoms (ii) with iodomethane and tBuOK in THF at 60°C results in benzimidazolium iodide, **1-I** in very good yield (>70%). **1-I** can be quantitatively reacted with appropriate silver salts through metathesis reaction thus giving **1-OTf** and **1-NO$_3$**. The high purity grade of the final products, required for photophysical measurements, are obtained by flash chromatography through the automated Biotage® system and multiple recrystallizations with proper solvents.

Solutions

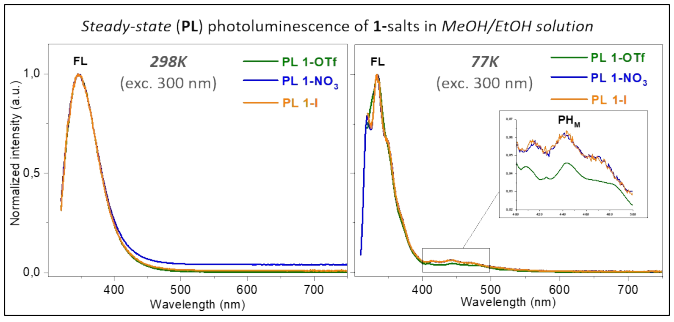

Figure 1. Emission spectra (300 nm excitation wavelength) of diluted solutions (10^{-5} M in MeOH/EtOH) of **1-OTf** (green), **1-NO$_3$** (blue) and **1-I** (orange).

Absorption spectra of **1**-salts in diluted solution of polar solvents (MeOH/EtOH 1:4) show three maxima at 210, 240 and 280 nm (Figure S4a). Similarly, the photoluminescence spectra (PL) at 298 K (λ_{exc}= 300 nm, see Table 1 and Figure 1 left) show intense fluorescence at 345 nm (lifetime, τ, 1.54-1.57 ns) with a slight variation of quantum yields among the three salts (Φ equal to 77.5, 52.6 and 53.6% for **1-OTf**, **1-NO$_3$** and **1-I** respectively). At 77 K (Figure 1 right), alongside the FL, a very weak structured phosphorescence emerges at about 450nm (τ_{av} >2 s, see Table 1 and Figure S5).

A combination of photophysical and NMR studies on diluted solutions of **1**-salts in low polar solvent has been performed in order to study the ion pairing effect. NMR studies of the three salts confirm an effect of the counterion on going from polar DMSO-d_6 (Figure S1) to non-polar $CDCl_3$ solutions (Figure S2) as also reported for π-twisted benzimidazolium chromophores.[25] In DMSO-d_6 all the ^1H-NMR signals of the three salts are superimposable, while in $CDCl_3$ the chemical shifts of hydrogens, adjacent to the imidazolium ring (*CH$_3$-N and Hc*), are affected by the nature of the counterion, in agreement with a tighter ion pair in the solvent with the lower dielectric constant.[26,27]

Likewise a bigger downfield shift of signals has been also reported for bromine-substituted N-alkylcarbazole as a result of strongest interaction between the halogen and nitrogen atoms in derivatives with shortest linkers.[23] In **1**-salts, an increase in the electronegative character of counterions results in a higher net positive charge of nitrogen atoms shifting the protons to lower fields. This agrees with the more deshielded *CH$_3$-N* and *Hc* protons of **1-I** compared to those of **1-NO$_3$** and **1-OTf**. To exclude any possible effect due to the low solubility of the salts in non-polar solvent, their ^1H-NMR spectra have been also recorded in $CDCl_3$ at the same concentration (10^{-5} M) as used for photophysical studies (Figure S2). In these conditions, ^1H-NMR spectra show the same deshielding trend as that displayed by more concentrated solutions (10^{-3} M). Very similar behavior was previously reported by some of us regarding the chemical shift of protons, in α position to the positively charged nitrogen atom, of various methyl-pyridinium salts recorded in $CDCl_3$.[28]

^1H-NMR spectra of the three samples have also been obtained from CD_3OD solutions (Figure S3). The *Hc* and *CH$_3$-N* signals of **1**-salts are affected by the specific ionic pair observed in $CDCl_3$ solutions (**1-I** > **1-NO$_3$** ≥ **1-OTf**) although to a lesser extent. This could reasonably suggest that the counterion still plays a role in influencing the photophysical properties in alcoholic solution by explaining the slight variation in the recorded quantum yields of the investigated salts in MeOH/EtOH diluted solutions. Accordingly, the differences in the optical properties become more prominent when the three compounds are dissolved in $CHCl_3$ (10^{-5}M). The same absorption bands (240 and 282 nm) are observed for the three salts in polar and non-polar solvents (figure S4a and S4b respectively), while the emissive properties are more significantly affected. A severe quenching of fluorescence intensities at 345 nm (Φ = 43.6, 3.4 and 1.7% for **1-OTf**, **1-NO$_3$** and **1-I** respectively) is flanked by long-lived (τ_{av} = 4.34-5.58 ms) components at 450 nm (Table 1 and Figure S6) which become visible in steady-state PL spectra under direct triplet-excitation at 350 nm (Figure S4c). Direct population of triplet states has been recently reported as a feasible way to bypass S_1-T_1 ISC and improve phosphorescence quantum efficiency[29] or as a means to visualize the phosphorescent emission when overwhelmed by fluorescence.[30] Being visible also in polar solvent at 77K, (Figure 1, right side) such a high energy long-lived emission is ascribed to molecular origin (PH_M)

as also corroborated by computational investigation (*vide infra*). Time-delayed spectra further show very weak phosphorescence emissions emerging over 500 nm (Figure S4c). Being such a low-energy emission attributed to supramolecular behaviors (PH_S), as discussed in the section related to solid-state, this is most likely due to the formation of nanoaggregates in non-polar solution. The switching on of PH_M in $CHCl_3$ solutions at room temperature suggests an easier singlet-triplet (S-T) intersystem crossing (ISC) by ion-pairing assistance. The drop of quantum efficiencies of **1**-salts in $CHCl_3$ suggests that the fluorescence quenching is strongly correlated with the closeness of the anion and its electronegative character (**I** > **NO_3** ≥ **OTf**). In agreement, the highest fluorescence quantum efficiency has been observed in **1-OTf** which is endowed with the weakest ion-pairing in solutions. The theoretical study well elucidates the PL characteristics observed for **1**-salts in solution. The simulated TDDFT absorption spectrum of the isolated cation **1** displays three bands at 193, 220 and 245 nm (see Figure S14 and Table S3 for the first singlet and triplet excitation energies). Its overall shape reproduces the experimental one collected in MeOH/EtOH (v/v 1/4) for the three salts (all displaying three absorptions at λ_{abs}=210, 240 and 280 nm), though the computed maxima are shifted towards slightly higher energies. The $S_0 \rightarrow S_1$ excitation (oscillator strength f=0.60) is mainly (75%) a HOMO→LUMO transition where both HOMO and LUMO are π orbitals delocalized on the whole molecule (Figure S15). Analysis of the first singlet and triplet states of **1** reveals the presence of a triplet level (T_7) of (π,π*) character just below S_1 (ΔE = 0.162 eV, 8 nm). Such small S-T energy gap could allow an otherwise forbidden ISC from the singlet (S_1) to the close triplet state (T_7) which decays to T_1 by internal conversion. This explains the observed molecular phosphorescence (from T_1) accompanying the fluorescence (from S_1) of luminogen **1** in MeOH/EtOH solution at 77K.

To explore a possible effect of the counterion on the electronic levels of **1**, calculations on the **1-OTf**, **1-NO_3** and **1-I** ionic pairs have also been carried out, starting from the respective X-ray structures of the three salts (see below) and freezing angles and torsions to preserve the relative arrangement of the ions as observed in the crystals (for **1-NO_3** the structure of **1-NO_3·H_2O** has been considered as starting point). The first significantly populated (i.e. with f>0.1) singlet excited state, despite its charge transfer (CT) character from the anion towards **1** (Figure S16), is only slightly shifted towards lower energies (248, 249 and 253 nm for **1-OTf**, **1-NO_3** and **1-I**, respectively, see Table S4) than that computed for **1** (245 nm), in accordance with the nearly superimposable absorption spectra recorded in polar and non-polar solutions. Looking at the closest triplet levels, it is found that the S-T energy gap further reduces from 0.162 (**1**) to 0.068 (both **1-OTf** and **1-NO_3** pairs) and 0.010 eV (**1-I**), triggering an even easier S-T ISC with respect to the isolated cation in accordance with FL quenching and PH_M enhancement observed in non-polar solvent. Notably, the lowest S-T energy gap calculated for **1-I** well agrees with the strongest electronegative character of iodide as evidenced by ^{1}H-NMR analysis.

Solid state

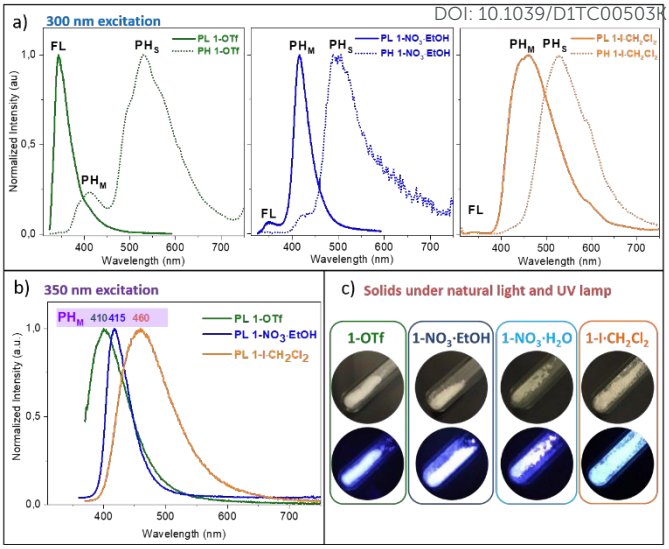

Figure 2. a) Steady state (solid line) and time-delayed (dotted line) photoluminescence emission at 300 nm excitation wavelength; b) steady-state photoluminescence emission at 350 nm excitation wavelength; c) photographs of **1**-salts powders under natural and UV light (366 nm).

In solid state, **1**-salts exhibit concomitant fluorescence and multiple phosphorescence emissions whose relative position, intensity and lifetime at room temperature are strongly dependent on the counterion and crystal features.

Four different crystalline phases have been isolated from acetonitrile/H_2O (**1-NO_3·H_2O**), ethanol (**1-OTf** and **1-NO_3·0.5EtOH**) and dichloromethane (**1-I·0.5CH_2Cl_2**). By exciting all crystals at 300 nm at room temperature, a fluorescent (τ in the ns regime, see Table 1 and Figures S7-11) emission at about 350 nm is observed together with phosphorescent components with properties depending on the specific anion and its relative distance from the cation (see Table 1, Figures 2 and S7a). In particular, while the steady-state spectrum of **1-OTf** (Figure 2a, solid-line) displays only an intense fluorescent emission (FL), the time-delayed spectrum (Figure 2a, dotted-line) reveals the presence of two phosphorescences at 410 nm (τ_{av} = 23.08 ms, PH_M) and 530 nm (τ_{av} = 327.33 ms, PH_S). Interestingly, for crystals of **1-NO_3·H_2O** and **1-NO_3·0.5EtOH** the PH_M component (at 415 nm, τ_{av} = 11.43 and 5.43 ms, respectively) is already observed in the steady-state spectrum together with the FL at 350 nm (see Figure 2a and S7a). An additional long-lived component PH_S can be detected at 530 nm (τ_{av} = 12.18 and 8.23 ms for **1-NO_3·H_2O** and **1-NO_3·0.5EtOH**, respectively) in the time-delayed spectra. The PL spectrum of **1-I·0.5CH_2Cl_2** displays an almost undetectable FL and an intense, broad phosphorescence band PH_M at 460 nm (τ_{av} = 6.15 ms). Again, PH_S is detected only in the delayed spectrum at 530 nm (τ_{av} = 15.03 ms). It is worth noting that the red shift of PH_M band observed in nitrate (5 nm) and iodide (50 nm) salts with respect to the one of triflate, follows the trend of electronegative character of the anions.

To disclose the effect of counterions on solid state photophysics, the crystal structures of the four salts have been determined by single crystal X-ray diffraction analysis. **1-OTf**, **1-NO_3** and **1-I** crystallize in the *P*-1 (**1-OTf** and **1-NO_3·H_2O**) and *C*2/*c* (**1-NO_3·0.5EtOH** and **1-I·0.5CH_2Cl_2**) space groups (see

View Article Online
DOI: 10.1039/D1TC00507K

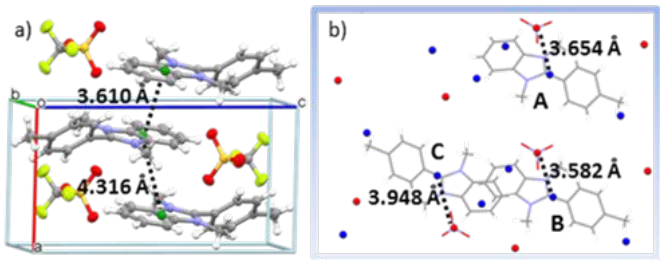

Figure 3. Fragment of crystal packing of (a) **1-OTf** with shortest distances between benzimidazole centroids (green circles) and (b) **1-NO_3·0.5EtOH** with shortest distances between cation and anion (blue and red circles, respectively) centroids for the three independent ionic pairs.

Figures 3 and S12). The asymmetric units of **1-NO_3·H_2O** and **1-I·0.5CH_2Cl_2** include one water and one-half dichloromethane cocrystallized molecule, respectively, while that of **1-NO_3·0.5EtOH** comprises three independent ionic pairs (labelled as A, B and C) and one and one-half ethanol cocrystallized molecule. XRD analysis shows that **1** is far from being planar, as indicated by the dihedral angle between the least-squares (l.s.) planes through the benzimidazole moiety and the phenyl ring, varying in the range 48.23-52.35° in the four structures.

The benzimidazole moiety forms in all cases stacks of head-to-tail π-π dimeric aggregates. Two independent stacks are found in the crystal structure of **1-NO_3·0.5EtOH**, one built up by A molecules and the other by B and C molecules. Along the stacks, the distances between benzimidazole centroids are alternately equal to 3.610 and 4.316 Å (**1-OTf**), 3.555 and 4.526 Å (**1-NO_3·H_2O**), 3.416/3.487 and 5.227/5.180 Å (**1-NO_3·0.5EtOH**, stacks A/B,C) and 3.566 and 4.767 Å (**1-I·0.5CH_2Cl_2**). The short distances between centroids suggest the presence of H-dimers owing to both the very little slippages (0.49, 0.46, 0.53 and 0.62 Å for **1-OTf**, **1-NO_3·H_2O**, **1-NO_3·0.5EtOH** and **1-I·0.5CH_2Cl_2**, respectively, considering, for **1-NO_3·0.5EtOH**, the H-dimer of A molecules) and the values of the angle θ between the centroid-centroid vector and its projection on the molecular plane (82, 83, 81 and 80° in the same order as above). Such H-dimers are laterally shifted along the stacks with much larger slippages (2.3, 2.8, 4.0 and 3.1 Å and θ = 58, 52, 40 and 49° for **1-OTf**, **1-NO_3·H_2O**, **1-NO_3·0.5EtOH** and **1-I·0.5CH_2Cl_2**, respectively). In all structures, the cations are laterally connected via $CF_3SO_3^-$ or NO_3^- or I^- anions through weak C–H···X (X=F, O in triflate; X=N, O in nitrates and X=I in iodide) hydrogen bonds (HB). The strongest interactions correspond to H···X distances/C–H···X angles of 2.45 Å/169° (X=O, **1-OTf**), 2.49 Å/177° (X=O, **1-NO_3·H_2O**), 2.36 Å/162° (X=O, **1-NO_3·0.5EtOH**) and 2.91 Å/170° (X=I, **1-I·0.5CH_2Cl_2**). In addition, in both nitrates structures the cocrystallized solvent molecules behave as HB donors of medium strength with oxygen atoms of NO_3^- anions. The CH_2Cl_2 cocrystallized molecule in **1-I**, on the other hand, is weakly hydrogen bonded to both **1** and I^-, in agreement with a slow loss of crystallinity at room temperature.

The separations between ionic pairs in the four structures (see Figure 3b for **1-NO_3·0.5EtOH** and Figure S13) reveal that the shorter distances between cation-anion centroids increase from 3.582 to 4.385, 4.596 and 5.296 Å moving from **1-NO_3·0.5EtOH** to **1-I·0.5CH_2Cl_2**, **1-NO_3·H_2O** and **1-OTf**, respectively. This trend clearly does not reproduce that expected from NMR investigation according to which the cation-anion distances should increase in the order **I** < **NO_3** ≤ **OTf** based only on electronegativity effect. In crystal state other factors come into play and result in the shortest value for **1-NO_3·0.5EtOH**. This is obviously imputable to the reduced dimensions of the counter-ion (compared to that of **1-OTf**) and of the cocrystallized solvent molecule (compared to that of **1-I·0.5CH_2Cl_2**) and to the 2:1 ratio between ionic pair and cocrystallized solvent molecule (compared to the 1:1 ratio in **1-NO_3·H_2O**). Thus, the strength of the ion pair concomitantly depends on the anion electronegativity and cation-anion distances and is expected to be reduced from the most electronegative iodide to the less electronegative and more distant triflate. However, the close proximity of nitrate to the cation could reasonably provide a reinforced ion-pairing in **1-NO_3·0.5EtOH**.

These analyses, together with theoretical calculations reported above, allow to justify the photophysical behavior of crystalline **1**-salts. The presence of heavy atom along with the narrowest S-T gap computed for **1-I·0.5CH_2Cl_2** well agree with an easier ISC, thus producing PH_M enhancement and concomitant FL quenching as a result of the strong EHE. On the other side, the **1-OTf** PL-spectrum shows only the FL band while in **1-NO_3** both FL and PH_M are displayed. Noticeably, the emissive patterns of **1-NO_3·0.5EtOH** and **1-NO_3·H_2O** salts, equipped with the same counter ion but with different anion-cation center of mass separation, show inverted ratio of FL and PH_M intensities (Figure S7a). **1-NO_3·H_2O** displays intense FL and weak PH_M while **1-NO_3·0.5EtOH** the opposite, confirming that the ion-pairing effect increases with reducing the distances between the ions thus making the ISC easier. Accordingly, by decreasing the ions distance, the quenching of fluorescence and the intensity of phosphorescence increase. Despite the co-crystallized solvent effect cannot be totally excluded, the impact of ions distance on photophysical properties of the same ionic couple has never been investigated to date.

As expected by a reinforced ion-pairing, the drop of fluorescence quantum efficiency in crystalline **1-OTf**, **1-NO_3·0.5EtOH**, **1-NO_3·H_2O** and **1-I·0.5CH_2Cl_2** follows a trend similar to that observed in $CHCl_3$ solutions (Φ equal to 51, 4, 2 and 11 %, respectively). The weak cation-anion interaction in **1-OTf** produces the highest quantum efficiency observed at 300 nm excitation and guarantees ultrabright FL emission both in solution and in solid state.

Concerning the low energy phosphorescence, PH_S, of the four salts, the single crystal XRD study allows to explain its origin as due to the presence of H-dimers in their crystal structure, as thoroughly demonstrated for other luminophores.[11,31]

The presence of cocrystallized solvent may play, as well, a role in the observed solid-state behavior introducing non radiative deactivation paths. In fact, shorter lifetimes are measured for **1-NO_3·H_2O** (12.18 ms), **1-NO_3·0.5EtOH** (8.23 ms) and **1-I·0.5CH_2Cl_2** (15.03 ms) crystals compared with that of the solvent free **1-OTf** salt (327.33 ms) which exhibits ultralong RTP with afterglow up to 2s. The different lifetimes of the two phosphorescence

View Article Online
DOI: 10.1039/D1TC00503K

emissions at room temperature allow to observe blue to green color variation with the naked eye (Figure 4).

Table 1. Photophysical properties of **1**-salts at room temperature and 77K.

Entry	SOLUTION		Entry	SOLID STATE			
	MeOH/EtOH	*$CHCl_3$*		*Crystal*		*Powder*	
1-OTf	Φ_{300} 77.5%	Φ_{300} 43.6%	**1-OTf**	Φ_{300} 50.7%	Φ_{350} 34.7%	Φ_{300} 57.9%	Φ_{350} 23.2%
FL	**345 nm -** 0.94 ns *1.54 ns[a]*	**345 nm -** 1.17 ns	**FL**	**345 nm -** 0.89 ns *0.94 ns[a]*			
PH_M	**450nm -** --[b] *2446.00 ms[a]*	**450 nm -** 4.59 ms	**PH_M**	**410 nm -** 23.08 ms *46.80 ms[a]*			
			PH_S	**530 nm -** 327.33 ms *1096.10 ms[a]*			
1-NO_3	Φ_{300} 52.6%	Φ_{300} 3.4%	**1-NO_3·EtOH**	Φ_{300} 3.7%	Φ_{350} 73%	Φ_{300} 2.2%	Φ_{350} 71%
FL	**345 nm -** 1.21 ns *1.57 ns[a]*	**345 nm -** 0.97 ns	**FL**	**345 nm -** 0.65 ns *0.66 ns[a]*			
PH_M	**450 nm -** --[b] *2230.30 ms[a]*	**450 nm -** 5.85 ms	**PH_M**	**415 nm -** 5.43 ms *29.26 ms[a]*			
			PH_S	**530 nm -** 8.23 ms *1104.40 ms[a]*			
			1-NO_3·H_2O	Φ_{300} 1.9%	Φ_{350} 25%	Φ_{300} 4.0%	Φ_{350} 34.4%
			FL	**345 nm -** 0.42 ns *0.76 ns[a]*			
			PH_M	**415 nm -** 11.43 ms *35.31 ms[a]*			
			PH_S	**530 nm -** 12.18 ms *1178.50 ms[a]*			
1-I	Φ_{300} 53.6%	Φ_{300} 1.7%	**1-I·CH_2Cl_2**	Φ_{300} 11.4%	Φ_{350} 23.7%	Φ_{300} 15.6%	Φ_{350} 26.1%
FL	**345 nm -** 1.20 ns *1.55 ns[a]*	**345 nm –** 1.05 ns	**FL**	**345 nm -** 0.45 ns *1.05 ns[a]*			
PH_M	**450nm -** --[b] *2232.60 ms[a]*	**450 nm -** 4.36 ms	**PH_M**	**460 nm -** 6.15 ms *59.08 ms[a]*			
			PH_S	**530 nm -** 15.03 ms *1145.50 ms[a]*			

[a] measurements conducted at 77K; [b] PH_M not detectable (only τ in *ns* timescale attributed to the intense FL component).

In agreement with the excitation spectra (Figure S7), the T_1 state of the four crystals can be directly populated by exciting at 350 nm. As stated above, the direct excitation of triplet-states allows to visualize the PH_M emission overwhelmed by the intense FL.[30] The corresponding PL emission spectrum of **1-OTf** crystals (Figure 2b), in fact, shows only PH_M at 410 nm (Φ_{350} = 34.7%). Similarly, the PL spectra of nitrate and iodide crystals exhibit their corresponding PH_M bands (Figure 2b) with a sizable enhancement of quantum efficiencies. Remarkably, **1-NO_3·0.5EtOH** crystals show impressively high phosphorescence quantum efficiency (Φ_{350} = 73%).[15,32] **1-NO_3·H_2O** and **1-I·0.5CH_2Cl_2** crystals exhibit a minor, still consistent, increase in their relative quantum yields (Φ_{350} = 25% and 23.7% respectively). Such an efficient direct population of the triplet state, reflecting in quantum yields above 20% in all crystals, is also evidenced by their bright luminescence under 366 nm lamp excitation (Figure 2c). Except for **1-OTf** which shows a lowering in the quantum efficiency when moving from 300 to 350 nm excitation wavelengths, most likely attributed to the loss of the intense FL emission, a boosted quantum yield is observed for **1-NO_3·0.5EtOH**, **1-NO_3·H_2O** and **1-I·0.5CH_2Cl_2** crystals. In agreement, these latter all show, at 350 nm excitation, higher ratios between radiative (K_r) and non-radiative rate constant (K_{nr}) than those obtained by exciting at 300 nm (Table S1).

Despite the presence of solvent molecules in the crystal packing, the direct triplet-excitation of **1-NO_3·0.5EtOH** crystals produces the highest phosphorescence quantum efficiency in the series. Considering the same counterion in **1-NO_3·0.5EtOH** and **1-NO_3·H_2O**, the former is characterized by the shorter distance between cation-anion centers of mass (3.582 vs. 4.596 Å), smaller non-radiative (K_{nr} = 50.00 vs. 65.56 s^{-1}) and greater

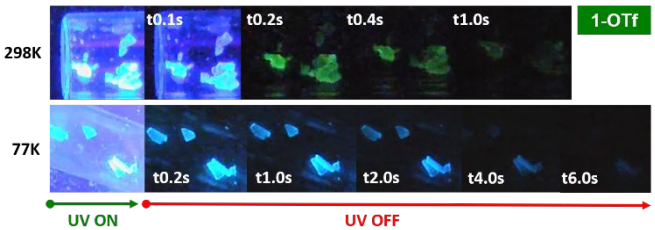

Figure 4. Afterglow of **1-OTf** crystals at 298K and 77K before and after ceasing UV excitation (366nm).

radiative (K_r = 135.19 vs. 21.85 s^{-1}) rate constants. Once again this supports the role played by the counterion and its vicinity to the luminophore in activating the phosphorescent emission. Further the differences in quantum efficiencies observed in the two nitrate salts under 350 nm excitation suggest that the stronger ion-pairing, the more efficient the direct triplet-excitation.

Crystallinity dependent optical responses

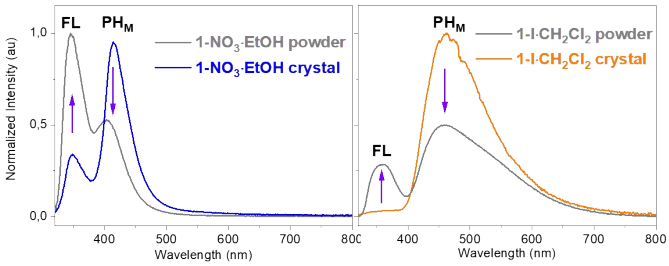

Figure 5. PL spectra of **1-NO_3·0.5EtOH** and **1-I·0.5CH_2Cl_2** solids before (blu and orange lines respectively) and after grinding (grey lines) (λexc=300 nm).

The multi-emissive patterns of **1**-salts vary upon mechanical stimuli produced by grinding of crystalline samples in an agata mortar. By excitation at 300 nm, ground **1-I** and **1-NO_3** (both forms) exhibit FL enhancement and PH_M quenching (Figure 5) but almost unchanged overall quantum efficiency. Ground **1-OTf** displays a slight increase of its only fluorescent emission (QY_{300} = 57.9%).

By 350 nm excitation, the effect of grinding on the isolated phosphorescent emission can be analyzed. Ground **1-OTf** shows a reduced QY_{350} (23.2%) with respect to that obtained in highly ordered crystals (34.7%). On the other hand, in **1-NO_3·0.5EtOH**, the variation of QY_{350} is almost negligible after mechanical micronization. Finally, an increased QY_{350} is observed for both ground **1-NO_3·H_2O** (Φ_{350} = 34.4%) and **1-I·0.5CH_2Cl_2** (Φ_{350} = 26.1%). Such variations could be ascribed to a number of factors including, for example, the partial loss of loosely packed cocrystallized solvent, the introduction of surface defects and the reduction of crystal sizes,[33–35] all of them affecting the photophysics of ground **1**-salts.

Conclusions

In this work we develop a facile strategy to manipulate the emissive properties of a new class of ionic luminogens, based on benzimidazolium ion **1** and prepared with different counterions, i.e. triflate, iodide and nitrate. The photophysical study along with theoretical calculations, single crystal X-ray diffraction analysis and *^1H*-NMR investigation, performed in diluted solutions of both polar and low polar solvents, have allowed to disclose the effect of counterion on molecular and supramolecular emissive properties of **1**-salts. Four crystals have been obtained, i.e., **1-OTf**, **1-I·0.5CH_2Cl_2**, **1-NO_3·H_2O** and **1-NO_3·0.5EtOH**. They display at room temperature multiple emissions, comprising fluorescence (FL), molecular phosphorescence (PH_M) and supramolecular phosphorescence (PH_S), the latter associated with the presence of strong π-π stacking interactions in the crystal structures. The position and relative intensities of these emissions are found to depend on the nature of counterion as a combination of ion-pairing effects and supramolecular interactions. In particular, crystals of **1-OTf**, displaying the weaker anion-cation interaction, provide ultrabright fluorescence and supramolecular long-lasting RTP; **1-I·0.5CH_2Cl_2** crystals mainly show molecular phosphorescence, promoted by the EHE of iodide counter-ion granting an efficient singlet-triplet ISC; nitrate salts, characterized by different cation-anion distances, exhibit simultaneously fluorescence and molecular phosphorescence. More specifically, crystals of **1-NO_3·H_2O** display intense FL and weak PH_M while those of **1-NO_3·0.5EtOH** the opposite. For the latter salt, having the shortest anion-cation distance within the series of examined compounds, an impressive phosphorescence quantum efficiency is obtained by direct population of the triplet states.

These findings clearly demonstrate that strong ion-pairing is associated with i) severe quenching of fluorescence; ii) enhancement of molecular phosphorescence by facilitating singlet-triplet ISC; iii) efficient direct population of triplet states. The supramolecular long-lasting RTP observed at lower energies appears to be less affected by the specific anion owing to the close similarity in the stacking pattern of the examined structures. The presence of co-crystallized solvent molecules, however, clearly affects the PH_S lifetimes, which are significantly longer for **1-OTf**, free from co-crystallized solvent molecules, than for the other salts.

The results obtained on the ion-pairing effects are expected to contribute to the understanding of the key-principles governing the emissive properties of ionic salts, providing a tool for the design of new luminescent ionic molecules with fine-tailored optical properties.

Author Contributions

G.D.C. and P.M. synthesized and characterized 1-salts. D.M. performed photophysical study. C.B. performed time-delayed spectroscopic investigation. A.F. performed crystallography and computational investigation. F.T. performed absorption spectra and data curation and M.P. was involved in editing processes. The project was conceived by E.C., A. F. and G.D.C. The manuscript was written by E.C., A. F. and G.D.C. All authors have given approval to the final version of the manuscript.

Conflicts of interest

There are no conflicts to declare.

Acknowledgements

The use of instrumentation purchased through the Regione Lombardia-Fondazione Cariplo joint SmartMatLab Project is gratefully acknowledged. G.D.C. greatly thanks the University of

Milan (Piano Sostegno alla Ricerca 2018 LINEA 2 Azione A - Giovani Ricercatori) for financial support.

References

1 S. Hirata, *Adv. Opt. Mater.*, 2017, **5**, 1700116.
2 S. Xu, Y. Duan and B. Liu, *Adv. Mater.*, 2020, **32**, 1903530.
3 F. Würthner, *Angew. Chemie Int. Ed.*, 2020, **59**, 14192–14196.
4 C.-R. Wang, Y.-Y. Gong, W.-Z. Yuan and Y.-M. Zhang, *Chinese Chem. Lett.*, 2016, **27**, 1184–1192.
5 A. Forni, E. Lucenti, C. Botta and E. Cariati, *J. Mater. Chem. C*, 2018, **6**, 4603–4626.
6 Kenry, C. Chen and B. Liu, *Nat. Commun.*, 2019, **10**, 2111.
7 E. Lucenti, A. Forni, C. Botta, L. Carlucci, C. Giannini, D. Marinotto, A. Pavanello, A. Previtali, S. Righetto and E. Cariati, *Angew. Chemie Int. Ed.*, 2017, **56**, 16302–16307.
8 W. Zhao, Z. He, J. W. Y. Lam, Q. Peng, H. Ma, Z. Shuai, G. Bai, J. Hao and B. Z. Tang, *Chem*, 2016, **1**, 592–602.
9 P. Alam, N. L. C. Leung, J. Liu, T. S. Cheung, X. Zhang, Z. He, R. T. K. Kwok, J. W. Y. Lam, H. H. Y. Sung, I. D. Williams, C. C. S. Chan, K. S. Wong, Q. Peng and B. Z. Tang, *Adv. Mater.*, 2020, **32**, 2001026.
10 Z. An, C. Zheng, Y. Tao, R. Chen, H. Shi, T. Chen, Z. Wang, H. Li, R. Deng, X. Liu and W. Huang, *Nat. Mater.*, 2015, **14**, 685–690.
11 E. Lucenti, A. Forni, C. Botta, L. Carlucci, C. Giannini, D. Marinotto, A. Previtali, S. Righetto and E. Cariati, *J. Phys. Chem. Lett.*, 2017, **8**, 1894–1898.
12 S. d'Agostino, F. Spinelli, P. Taddei, B. Ventura and F. Grepioni, *Cryst. Growth Des.*, 2019, **19**, 336–346.
13 A. S. Carretero, A. S. Castillo and A. F. Gutiérrez, *Crit. Rev. Anal. Chem.*, 2005, **35**, 3–14.
14 H. Shi, Z. An, P.-Z. Li, J. Yin, G. Xing, T. He, H. Chen, J. Wang, H. Sun, W. Huang and Y. Zhao, *Cryst. Growth Des.*, 2016, **16**, 808–813.
15 G. Chen, S. Guo, H. Feng and Z. Qian, *J. Mater. Chem. C*, 2019, **7**, 14535–14542.
16 Y. Li, Y. Lei, L. Dong, L. Zhang, J. Zhi, J. Shi, B. Tong and Y. Dong, *Chem. – A Eur. J.*, 2019, **25**, 573–581.
17 W. Xi, J. Yu, M. Wei, Q. Qiu, P. Xu, Z. Qian and H. Feng, *Chem. – A Eur. J.*, 2020, **26**, 3733–3737.
18 Z. Cheng, H. Shi, H. Ma, L. Bian, Q. Wu, L. Gu, S. Cai, X. Wang, W. Xiong, Z. An and W. Huang, *Angew. Chemie Int. Ed.*, 2018, **57**, 678–682.
19 J. Wang, X. Gu, H. Ma, Q. Peng, X. Huang, X. Zheng, S. H. P. Sung, G. Shan, J. W. Y. Lam, Z. Shuai and B. Z. Tang, *Nat. Commun.*, 2018, **9**, 2963.
20 G. Chen, H. Feng, F. Feng, P. Xu, J. Xu, S. Pan and Z. Qian, *J. Phys. Chem. Lett.*, 2018, **9**, 6305–6311.
21 G. Zhang, X. Zhang, L. Kong, S. Wang, Y. Tian, X. Tao and J. Yang, *Sci. Rep.*, 2016, **6**, 37609.
22 J. Wang, X. Gu, P. Zhang, X. Huang, X. Zheng, M. Chen, H. Feng, R. T. K. Kwok, J. W. Y. Lam and B. Z. Tang, *J. Am. Chem. Soc.*, 2017, **139**, 16974–16979.
23 X. Sun, B. Zhang, X. Li, C. O. Trindle and G. Zhang, *J. Phys. Chem. A*, 2016, **120**, 5791–5797.
24 S. Riera-Galindo, A. Orbelli Biroli, A. Forni, Y. Puttisong, F. Tessore, M. Pizzotti, E. Pavlopoulou, E. Solano, S. Wang, G. Wang, T.-P. Ruoko, W. M. Chen, M. Kemerink, M. Berggren, G. di Carlo and S. Fabiano, *ACS Appl. Mater. Interfaces*, 2019, **11**, 37981–37990.
25 A. J.-T. Lou, S. Righetto, E. Cariati and T. J. Marks, *Chem. – A Eur. J.*, 2018, **24**, 15801–15805.
26 F. Tessore, D. Roberto, R. Ugo, P. Mussini, S. Quici, I. Ledoux-Rak and J. Zyss, *Angew. Chemie Int. Ed.*, 2003, **42**, 456–459.
27 F. Tessore, D. Locatelli, S. Righetto, D. Roberto, R. Ugo and P. Mussini, *Inorg. Chem.*, 2005, **44**, 2437–2442.
28 F. Tessore, E. Cariati, F. Cariati, D. Roberto, R. Ugo, P. Mussini, C. Zuccaccia and A. Macchioni, *ChemPhysChem*, 2010, **11**, 495–507.
29 J. Yuan, R. Chen, X. Tang, Y. Tao, S. Xu, L. Jin, C. Chen, X. Zhou, C. Zheng and W. Huang, *Chem. Sci.*, 2019, **10**, 5031–5038.
30 E. Lucenti, A. Forni, A. Previtali, D. Marinotto, D. Malpicci, S. Righetto, C. Giannini, T. Virgili, P. Kabacinski, L. Ganzer, U. Giovanella, C. Botta and E. Cariati, *Chem. Sci.*, 2020, **11**, 7599–7608.
31 A. Previtali, E. Lucenti, A. Forni, L. Mauri, C. Botta, C. Giannini, D. Malpicci, D. Marinotto, S. Righetto and E. Cariati, *Molecules*, 2019, **24**, 2552.
32 A. Fermi, G. Bergamini, R. Peresutti, E. Marchi, M. Roy, P. Ceroni and M. Gingras, *Dye. Pigment.*, 2014, **110**, 113–122.
33 A. Patra, N. Hebalkar, B. Sreedhar, M. Sarkar, A. Samanta and T. P. Radhakrishnan, *Small*, 2006, **2**, 650–659.
34 T. Han, Y. Hong, N. Xie, S. Chen, N. Zhao, E. Zhao, J. W. Y. Lam, H. H. Y. Sung, Y. Dong, B. Tong and B. Z. Tang, *J. Mater. Chem. C*, 2013, **1**, 7314–7320.
35 C. Botta, S. Benedini, L. Carlucci, A. Forni, D. Marinotto, A. Nitti, D. Pasini, S. Righetto and E. Cariati, *J. Mater. Chem. C*, 2016, **4**, 2979–2989.